



# Identification of 14 Known Drugs as Inhibitors of the Main Protease of SARS-CoV-2

Mohammad M. Ghahremanpour, Julian Tirado-Rives, Maya Deshmukh, Joseph A. Ippolito, Chun-Hui Zhang, Israel Cabeza de Vaca, Maria-Elena Liosi, Karen S. Anderson,\* and William L. Jorgensen\*

**Cite This:** *ACS Med. Chem. Lett.* 2020, 11, 2526–2533

**Read Online**

ACCESS |

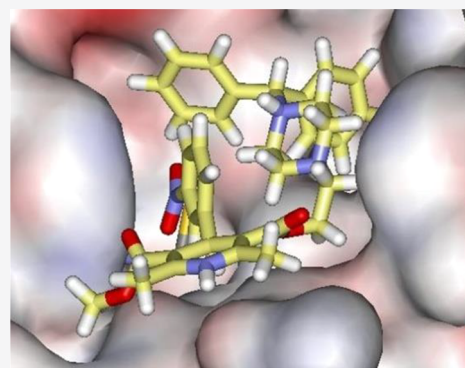
Metrics & More

Article Recommendations

Supporting Information

**ABSTRACT:** A consensus virtual screening protocol has been applied to ca. 2000 approved drugs to seek inhibitors of the main protease ( $M^{pro}$ ) of SARS-CoV-2, the virus responsible for COVID-19. 42 drugs emerged as top candidates, and after visual analyses of the predicted structures of their complexes with  $M^{pro}$ , 17 were chosen for evaluation in a kinetic assay for  $M^{pro}$  inhibition. Remarkably 14 of the compounds at 100- $\mu$ M concentration were found to reduce the enzymatic activity and 5 provided  $IC_{50}$  values below 40  $\mu$ M: manidipine (4.8  $\mu$ M), boceprevir (5.4  $\mu$ M), lercanidipine (16.2  $\mu$ M), bedaquiline (18.7  $\mu$ M), and efonidipine (38.5  $\mu$ M). Structural analyses reveal a common cloverleaf pattern for the binding of the active compounds to the P1, P1', and P2 pockets of  $M^{pro}$ . Further study of the most active compounds in the context of COVID-19 therapy is warranted, while all of the active compounds may provide a foundation for lead optimization to deliver valuable chemotherapeutics to combat the pandemic.

**KEYWORDS:** SARS-CoV-2, virtual screening, drug repurposing, protease inhibitors



SARS-CoV-2, the cause of the COVID-19 pandemic,<sup>1</sup> is a coronavirus (CoV) from the *Coronaviridae* family. Its RNA genome is ~82% identical to that of SARS-CoV,<sup>2</sup> which was responsible for the severe acute respiratory syndrome (SARS) pandemic in 2003.<sup>3</sup> SARS-CoV-2 encodes two cysteine proteases: the chymotrypsin-like cysteine or main protease, known as 3CL $^{pro}$  or  $M^{pro}$ , and the papain-like cysteine protease, PL $^{pro}$ . They catalyze the proteolysis of polyproteins translated from the viral genome into nonstructural proteins essential for packaging the nascent virion and viral replication.<sup>4</sup> Therefore, inhibiting the activity of these proteases would impede the replication of the virus.  $M^{pro}$  processes the polyprotein 1ab at multiple cleavage sites. It hydrolyzes the Gln-Ser peptide bond in the Leu-Gln-Ser-Ala-Gly recognition sequence. This cleavage site in the substrate is distinct from the peptide sequence recognized by other human cysteine proteases known to date.<sup>5</sup> Thus,  $M^{pro}$  is viewed as a promising target for anti SARS-CoV-2 drug design; it has been the focus of several studies since the pandemic has emerged.<sup>2,4–7</sup>

An X-ray crystal structure of  $M^{pro}$  reveals that it forms a homodimer with a 2-fold crystallographic symmetry axis.<sup>2,5</sup> Each protomer, with a length of 306 residues, is made of three domains (I–III). Domains II and I fold into a six-stranded  $\beta$ -barrel that harbors the active site.<sup>2,4,5</sup> Domain III forms a cluster of five antiparallel  $\alpha$ -helices that regulates the dimerization of the protease. A flexible loop connects domain II to domain III. The  $M^{pro}$  active site contains a Cys-His catalytic dyad and canonical

binding pockets that are denoted P1, P1', P2, P3, and P4.<sup>2</sup> The amino acid sequence of the active site is highly conserved among coronaviruses.<sup>8</sup> The catalytic dyad residues are His41 and Cys145, and residues involved in the binding of substrates include Phe140, His163, Met165, Glu166, and Gln189 (Figure 1). These residues have been found to interact with the ligands cocrystallized with  $M^{pro}$  in different studies.<sup>2,4,5</sup> Crystallographic data also suggested that Ser1 of one protomer interacts with Phe140 and Glu166 of the other as the result of dimerization.<sup>2,4</sup> These interactions stabilize the P1 binding pocket; thereby, dimerization of the main protease is likely for its catalytic activity.<sup>2,4</sup>

Drug repurposing is an important strategy for immediate response to the COVID-19 pandemic.<sup>9</sup> In this approach, the main goal of computational and experimental studies has been to find existing drugs that might be effective against SARS-CoV-2. For instance, a molecular docking study suggested remdesivir as a potential therapeutic that could be used against SARS-CoV-2,<sup>10</sup> which was supported experimentally by an  $EC_{50}$  value of 23

**Received:** September 28, 2020

**Accepted:** October 21, 2020

**Published:** October 25, 2020



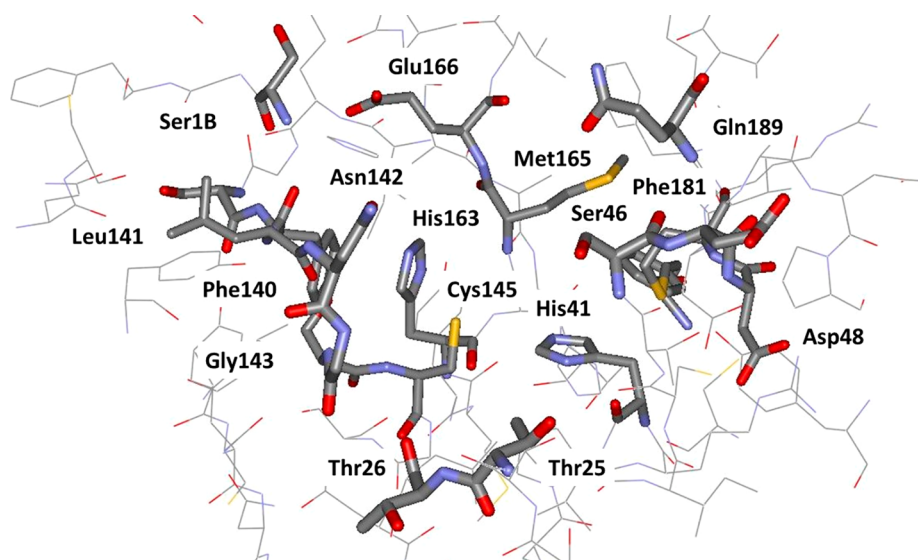


**Figure 1.** Rendering of the residues near the catalytic site of M<sup>Pro</sup> from a crystal structure at 1.31-Å resolution (PDB ID: 5R82). The catalytic residues are His41 and Cys145.

$\mu\text{M}$  in an infected-cell assay.<sup>11</sup> However, a clinical trial showed no statistically significant clinical benefits of remdesivir on adult patients hospitalized for severe COVID-19.<sup>12</sup> Nonetheless, patients who were administered remdesivir in the same trial showed a faster time to clinical improvement in comparison to the placebo-control group.<sup>12</sup> An  $\text{EC}_{50}$  value of 27  $\mu\text{M}$  was also reported for lopinavir,<sup>11</sup> suggesting it may have beneficial activity against SARS-CoV-2. However, neither lopinavir nor the lopinavir/ritonavir combination has thus far shown any significant benefits against COVID-19 in clinical trials. Chloroquine, hydroxychloroquine, and favipiravir have also been explored for repurposing against COVID-19; however, clinical studies with them have been controversial.<sup>13–16</sup> These studies reflect the urgent need for systematic drug discovery efforts for therapies effective against SARS-CoV-2.

Thus, we decided to pursue discovery of small-molecule inhibitors of M<sup>Pro</sup>. The aim of this initial work was 2-fold: to identify known drugs that may be inhibitors, but also to identify structurally promising, synthetically accessible substructures suitable for subsequent lead optimization. Our expectation was that existing drugs may show activity but not at the low-nanomolar levels that are typical of effective therapies.<sup>17</sup> This report provides results for the first goal. The work began by designing and executing a consensus molecular docking protocol to virtually screen  $\sim 2000$  approved drugs. The predicted structures (poses) of the complexes for the top-scoring 42 drugs received extensive scrutiny including consideration of intermolecular contacts, conformation, stability in molecular dynamics (MD) simulations, and potential for synthetic modification to arrive at 17 drugs, which were purchased and assayed for inhibition of M<sup>Pro</sup>. The outcome was strikingly successful with 14 of the 17 compounds showing some reduction of M<sup>Pro</sup> activity at 100  $\mu\text{M}$  concentration, and with 5 compounds yielding  $\text{IC}_{50}$  values below 40  $\mu\text{M}$ .

To begin, our analyses of more than 50 crystal structures of SARS-CoV-2 main protease in apo and holo forms showed small structural variations in the active site region. The overall root-mean-square deviation (RMSD) of all structures was  $\sim 0.8$  Å for  $\text{C}_\alpha$  atoms. The presence of a ligand in the crystal structure likely places the side chains of the active site residues in positions that

are more suitable for performing molecular docking compared to the apo form of the enzyme. Thus, we chose to use a high-resolution (1.31 Å) structure of M<sup>Pro</sup> cocrystallized with a noncovalent small fragment hit (PDB ID 5R82)<sup>18</sup> for docking the approved drugs after removal of the fragment (Figure 1). The program Reduce<sup>19</sup> was run on the structure for allowing side-chain flips, optimizing hydrogen bonds, and adding/removing hydrogen atoms. The pKa values of the ionizable residues of M<sup>Pro</sup> were predicted using the PROPKA3<sup>20</sup> and the H++ servers.<sup>21,22</sup> Accordingly, lysines and arginines were positively charged, aspartic and glutamic acids were negatively charged, and all histidines were neutral. All histidines were built with the proton on N $\epsilon$  except for His80, which was protonated at N $\delta$ . The resulting M<sup>Pro</sup> structure has a net charge of  $-4 e$ . Extensive visual inspection was carried out using UCSF Chimera.<sup>23</sup>

The next step was to pursue virtual screening by docking. Most docking programs apply methods to generate an initial set of conformations and tautomeric and protonation states for each ligand. This is followed by application of search algorithms and scoring functions to generate and score the poses of the ligand in the binding site of a protein. Scoring functions have been trained to reproduce a finite set of experimental ligand-binding affinities that are generally a mix of activity data converted to a free-energy scale. Therefore, the accuracy of the scores is dependent on multiple factors including the compounds that were part of the training set. To mitigate the biases, we performed four independent runs of protein–ligand docking with an in-house library of ca. 2000 approved, oral drugs using Glide SP, AutoDock Vina, and two protocols with AutoDock 4.2. The results were compiled, and further consideration focused on those compounds that ranked among the top 10% percent in at least 3 out of the 4 runs. The details of the docking protocols, correlations of docking scores, and the names and scores for all docked compounds are provided in the Supporting Information.

Molecular dynamics simulations were also performed starting from the Glide docking poses for the complexes of 14 high-interest compounds using the GROMACS software, version 2018a.<sup>24</sup> The protonated M<sup>Pro</sup> dimer, with a net charge of  $-8 e$ , was represented by the OPLS-AA/M force field.<sup>25</sup> TIP4P water

Table 1. Consensus Count (CC), Indication and Mechanism of Action of the Top 42 Drugs Selected from Virtual Screening<sup>a</sup>

Compound	CC	Indication	Mechanism of Action	Compound	CC	Indication	Mechanism of Action
avatrombopag maleate	3	Thrombocytopenia	Thrombopoietin receptor agonist	lurasidone	4	Schizophrenia	Dopamine D <sub>2</sub> receptor antagonist
azelastine	4	Allergic rhinitis	Histamine H <sub>1</sub> -receptors antagonist	macimorelin	3	Adult growth hormone deficiency	Ghrelin receptor agonist
azilsartan Medoxomil	4	Hypertension	Angiotensin II receptor antagonist	<b>manidipine</b>	3	Hypertension	Calcium channel blocker
<b>bedaquiline</b>	3	Tuberculosis	ATP synthase inhibitor	metergoline	4	Psychosis	Dopamine agonist
benzquercin	4	Inflammation	Flavonoid drug	methoserpidine	3	Hypertension	Monoamine transport inhibitor
<b>boceprevir</b>	3	Hepatitis C	Protease inhibitor	naldemedine	3	Opioid induced constipation	Opioid receptor antagonist
bromocriptine	4	Hyperprolactinemic disorders	Dopamine D <sub>2</sub> receptor agonist	<b>nelfinavir</b>	3	HIV infection	Protease inhibitor
<b>cabergoline</b>	4	Hyperprolactinemic disorders	Dopamine D <sub>2</sub> receptor agonist	nicomol	3	Hyperlipidemia	-
carindacillin	4	Bacterial infection	Penicillin-binding protein	nicomorphine	4	Analgesic	Opioid agonist
<b>cinnoxicam</b>	4	Inflammation	Prostaglandin synthesis inhibitor	nilotinib	4	Chronic myeloid leukemia	Kinase inhibitor
<b>clofazimine</b>	4	Lepromatous leprosy	Destabilizing bacterial membrane	<b>perampanel</b>	4	Partial-onset seizures	Glutamate receptor antagonist
dextetamide	3	Neuroleptic parkinsonism	Muscarinic antagonist	<b>periciazine</b>	3	Psychosis	Dopamine D <sub>1</sub> receptor antagonist
dihydroergocristine	4	Peripheral vascular disease	Serotonin receptors antagonist	pipamazine	3	Psychosis	Dopamine receptor antagonist
dihydroergocryptine	4	Parkinson's disease	Dopamine receptor agonist	saquinavir	4	HIV infection	Protease inhibitor
<b>efonidipine</b>	4	Hypertension	Calcium channel blocker	simvastatin	3	Hyperlipidemia	HMG-CoA reductase inhibitor
elbasvir	3	Hepatitis C	Protein 5A inhibitor	<b>talampicillin</b>	3	Antibacterial	Cell-wall synthesis inhibitor
<b>idarubicin</b>	4	Acute myeloid leukemia	Topoisomerase II inhibitor	telaprevir	3	Hepatitis C	Protease inhibitor
<b>indinavir</b>	3	HIV infection	Protease inhibitor	<b>tipranavir</b>	3	HIV infection	Protease inhibitor
ketoconazole	3	Fungal infection	14- $\alpha$ -sterol demethylase inhibitor	tropesin	3	Inflammation	Prostaglandin synthesis inhibitor
<b>lapatinib</b>	4	Breast and lung cancer	Kinase inhibitor	zafirlukast	4	Asthma	Leukotriene receptor antagonist
<b>lercanidipine</b>	4	Hypertension	Calcium channel blocker				
lomitapide	3	Hypercholesterolemia	Triglyceride transfer inhibitor				

<sup>a</sup> Assayed compounds are in bold.

was used as the solvent.<sup>26</sup> Sodium counterions were added to neutralize the net charge of each system. The selected ligand candidates were represented by the OPLS/CM1A force field,<sup>27</sup> as assigned by the BOSS software<sup>28</sup> (version 4.9) and the LigParGen Python code.<sup>29</sup> For neutral ligands, the CM1A partial atomic charges were scaled by a factor of 1.14.<sup>27</sup> Each M<sup>Pro</sup>-ligand complex was placed at the center of a triclinic simulation box with 10-Å padding. For each complex, several ns of equilibration were followed by a 70 ns unrestrained MD run in the NPT ensemble at 310 K and 1 atm. Further details are provided in the [Supporting Information](#).

On the experimental side, expression and purification of SARS-CoV-2 M<sup>Pro</sup> used a PGEX-6p-1 vector containing the gene for SARS-CoV-2 M<sup>Pro</sup> harboring a His<sub>6</sub> tag followed by a modified PreScission cleavage site to produce recombinant protein, as previously described.<sup>5</sup> Kinetic assays of SARS-CoV-2 M<sup>Pro</sup> activity were performed with compounds obtained from commercial sources except cinnoxicam, which had to be synthesized, and had purity >95% based on HPLC analysis. The kinetic measurements followed known procedures;<sup>5,7</sup> 100 nM M<sup>Pro</sup> in reaction buffer (20 mM Tris, 100 mM NaCl, 1 mM DTT, pH 7.3) was incubated with or without compound in DMSO at varying concentrations to a final DMSO concentration of 6% for 15 min with shaking at room temperature. The reaction was initiated by addition of substrate (Dabcyl-KTSAVLQ↓SGFRKM-E(Edans-NH<sub>2</sub>); GL Biochem) in reaction buffer, which is cleaved by M<sup>Pro</sup>, generating a product

containing a free Edans group. Fluorescence was monitored at an excitation wavelength of 360 nm and emission wavelength of 460 nm. Intrinsic fluorescence of the FRET substrate in reaction buffer alone or in the presence of each compound was monitored simultaneously and subtracted from the kinetic measurements of M<sup>Pro</sup>-mediated substrate cleavage. Measurements from control wells subtracted from those of experimental wells, measuring cleavage of substrate by M<sup>Pro</sup> in the absence of any compound, contained 50  $\mu$ M substrate with 6% DMSO in reaction buffer. For cleavage of substrate by M<sup>Pro</sup> in the presence of compound, the wells contained 50  $\mu$ M substrate and compound at a concentration corresponding to a final DMSO concentration of 6% in reaction buffer. Baseline subtraction controlled for intrinsic fluorescence of each compound as well as intrinsic fluorescence of the uncleaved FRET substrate. All measurements were performed in triplicate and averaged.

The results from the virtual screening were the predicted poses for the complexes and docking scores (in kcal/mol) that ranged from −10.85 to −0.59 for Glide, from −12.33 to −2.30 for AutoDock run 1, from −10.74 to −0.40 for AutoDock run 2, and from −8.50 to −2.10 for AutoDock Vina. As expected, the range of scores is wide and it is different from one docking program to another. The complete list of compounds and scores is provided in the [SI](#). Compounds were ranked based on their docking scores, and the top 200 hits from the four docking runs were compared. As the result, 42 compounds with a consensus count of 4 or 3 were selected. This means that these compounds



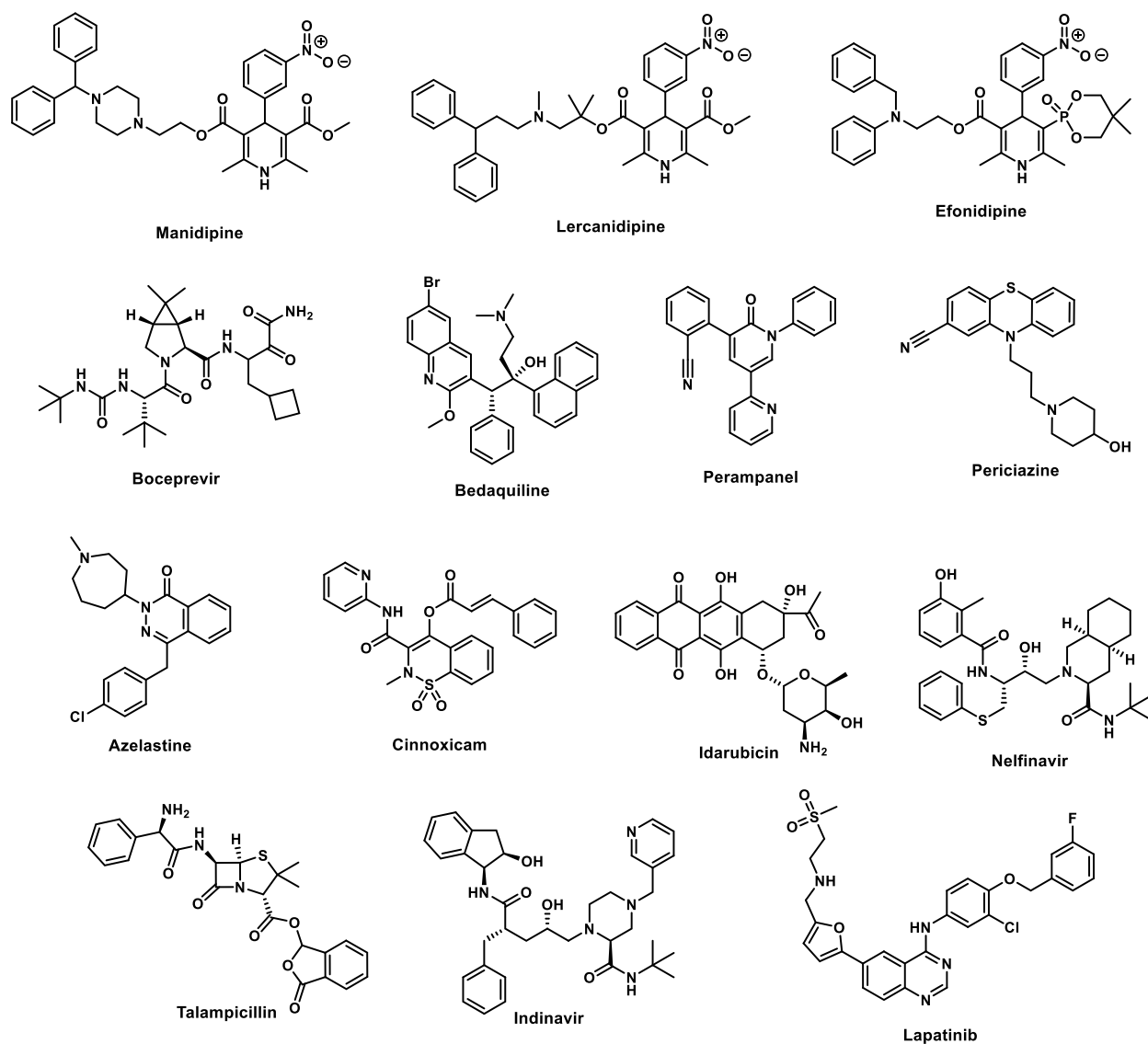


Figure 2. Selected high-scoring compounds from the consensus docking.

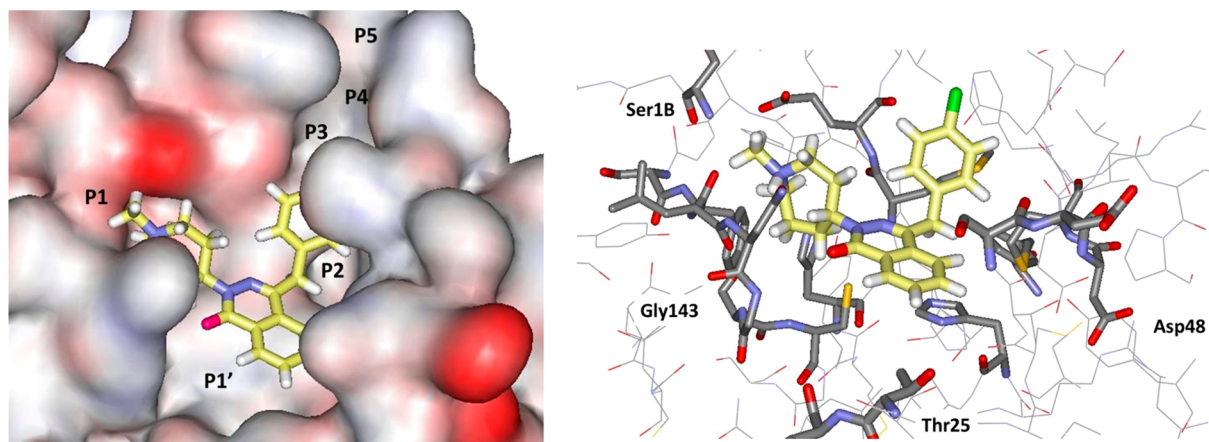
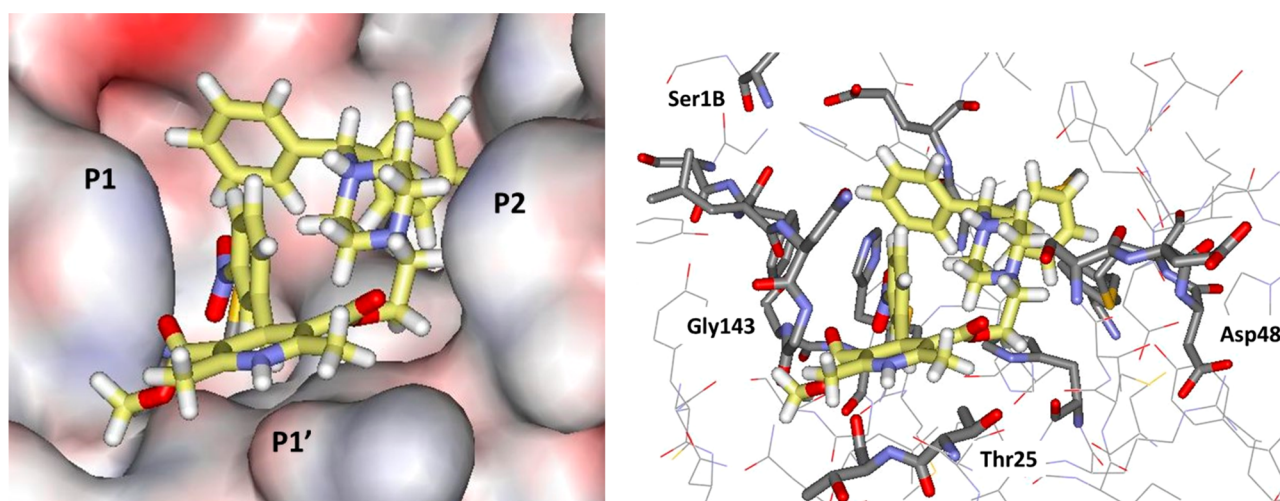


Figure 3. Glide docking pose for azelastine in surface (left; coloring by element) and stick (right) renderings. All illustrations are oriented with the P1 pocket to the left and P2 to the right, and all carbon atoms of ligands are in yellow.

were among the top-200 ranked compounds in all 4 or at least 3 out of the 4 docking runs. The indications and mechanisms of action for the 42 drugs are shown in Table 1, and the structures

of some of the ones that turned out to be most interesting are shown in Figure 2. The primary indications include bacterial and viral infections, hypertension, psychosis, inflammation, and



**Figure 4.** Glide docking pose for manidipine in surface (left) and stick (right) renderings.

cancer. Their mechanisms of action are also broad ranging from kinase and protease inhibitors to dopamine receptors agonists/antagonists and calcium channel blockers. It is not surprising that peptidic protease inhibitors are well-represented in view of the peptide substrate and prior discovery of peptidic inhibitors for  $M^{pro}$  and its SARS-CoV relative.<sup>7,30,31</sup>

In almost all cases the predicted poses for the 42 compounds from the different docking programs agreed well. The poses from Glide were then subjected to extensive visual scrutiny to check for unsatisfied hydrogen-bonding sites, electrostatic mismatches, and unlikely conformation of the ligand. About half of the compounds were ruled out for further study due to the occurrence of such liabilities and the presence of multiple ester groups (e.g., methoserpidine and nicomol) or overall size and complexity (e.g., bromocriptine and benzquercin). The MD simulations were carried out for 14 compounds to check the stability of the docked structures; this contributed to ruling out metergoline and dihydroergocristine that showed above normal drift without return, and it raised suspicion about talampicillin.

A repeated motif was apparent with high-scoring ligands having a cloverleaf pattern with occupancy of the P1, P1', and P2 pockets, as illustrated, for example, in Figure 3 for the complex of azelastine. Other common elements are an edge-to-face aryl–aryl interaction with His41 and placement of a positively charged group in the P1 pocket in proximity to Glu166, e.g., the methylazepanium group of azelastine, the protonated trialkylamino group of bedaquiline, and the protonated piperazine of pericizazine. However, Glu166 forms a salt-bridge with the terminal ammonium group Ser1B (Figure 1). The electrostatic balance seems unclear in this region, so our final selections included a mix of neutral and positively charged groups for the P1 site. The analysis of the high-scoring 42 compounds also considered structural variety and potential synthesis of analogs. In the end, we settled on 17 compounds, which are highlighted in Table 1, for purchase and assaying. Sixteen were commercially available, mostly from Sigma-Aldrich. The 17th, cinnoxamicam, was not available, but it was prepared in a one-step synthesis from the commercially available ester components. It may be noted that three calcium channel blockers, efonidipine, lercanidipine, and manidipine, were purchased (Figure 2). This was not done owing to the characteristic dihydropyridine substructure, since this end of the molecule protrudes out of the P1' site in the docked poses. It was for the variety in the left-sides

of the molecules in Figure 2, which form the cloverleaf that binds in the P1, P1', and P2 pockets, as illustrated in Figure 4 for manidipine. The steric fit in this region appears good with the two phenyl rings in the P1 and P2 sites, though the only potential hydrogen bond is between the nitro group and the catalytic Cys145.

The 17 known drugs were then evaluated using the FRET-based assay monitoring the fluorescence generated from the cleavage of a peptide substrate harboring an Edans–Dabcyl pair by recombinant SARS-CoV-2  $M^{pro}$ . Remarkably, 14 of the drugs at 100  $\mu$ M decreased  $M^{pro}$  activity (100 nM), as shown in Figure 5 and Table 2. Five drugs decreased  $M^{pro}$  activity to below 40%:

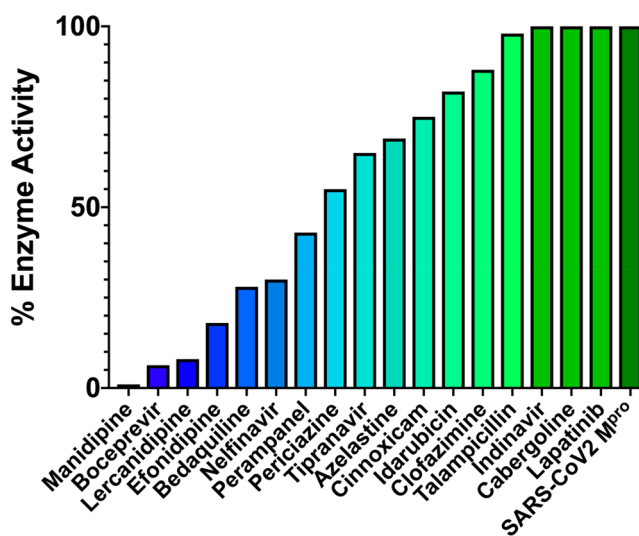


**Figure 5.** Ranking of the 17 compounds by percent residual enzyme activity monitored by cleavage product fluorescence following a 1 h incubation of 100 nM  $M^{pro}$  with 100  $\mu$ M compound. Compounds are ranked from most (blue) to least (green) active.

manidipine, boceprevir, efonidipine, lercanidipine, and bedaquiline. Dose–response curves were obtained to determine  $IC_{50}$  values, when possible, as shown in Figure 6 for the five most potent inhibitors, with the raw data as a function of time and concentration given in Figure S3.

The calcium channel-blockers manidipine, lercanidipine, and efonidipine inhibit  $M^{pro}$  activity with  $IC_{50}$  values of 4.8  $\mu$ M, 16.2

**Table 2.** Measured Activities of the 17 Compounds Tested for Inhibition of M<sup>pro</sup>

Compound	% Activity at 100 $\mu$ M	IC <sub>50</sub> ( $\mu$ M)
manidipine	1	4.81 $\pm$ 1.87
boceprevir	6	5.40 $\pm$ 1.53
lercanidipine	8	16.2 $\pm$ 2.94
efonidipine	18	38.5 $\pm$ 0.41
bedaquiline	28	18.7 $\pm$ 4.20
perampanel	43	100–250 <sup>a,b</sup>
periciazine	55	250 <sup>a</sup>
nelfinavir	64	250–600 <sup>a</sup>
tipranavir	65	>600 <sup>a</sup>
azelastine	69	20–100 <sup>a</sup>
cinnoxicam	75	>600 <sup>a</sup>
idarubicin	82	250–600 <sup>a</sup>
clofamizine	88	>600 <sup>a</sup>
talampicillin	90	250–600 <sup>a</sup>
indinavir	100	NA
cabergoline	100	NA
lapatinib	100	NA

<sup>a</sup>Estimate due to incomplete inhibition at 600  $\mu$ M. <sup>b</sup>Fluorescence of compound interfered with assay.

$\mu$ M, and 38.5  $\mu$ M, respectively. As suggested from Figure 4, the variation likely arises primarily from differences in binding of the left sides of the molecules (Figure 2) in the P1, P1', and P2 pockets. It has previously been proposed that such compounds might be useful for treatment of SARS-CoV-2 infection for their role as calcium channel blockers, not as M<sup>pro</sup> inhibitors.<sup>32</sup> Boceprevir, a hepatitis C virus protease inhibitor, inhibits M<sup>pro</sup> with an IC<sub>50</sub> of 5.4  $\mu$ M; its IC<sub>50</sub> has been previously reported as 4.13  $\mu$ M.<sup>7</sup> Bedaquiline, approved for the treatment of multidrug-resistant tuberculosis, inhibits M<sup>pro</sup> with an IC<sub>50</sub> of 18.7  $\mu$ M. The IC<sub>50</sub> of nelfinavir, an HIV protease inhibitor, was estimated to be between 250 and 600  $\mu$ M. Vatansever et al. have reported an IC<sub>50</sub> for nelfinavir of 234  $\mu$ M.<sup>33</sup> The other 12 compounds have not been previously reported as M<sup>pro</sup> inhibitors to our knowledge. Perampanel appears to be the sixth most active compound at 100  $\mu$ M, though its IC<sub>50</sub> could not be calculated

reliably, as its intrinsic fluorescence interfered with the fluorescence measurements.

The computed structures for the complexes of bedaquiline and boceprevir are illustrated in Figure 7. For bedaquiline, the three pockets are occupied by the ammonium containing side chain, the phenyl group, and the naphthyl group, respectively, while the quinoline fragment extends toward the solvent, and there are no clear protein–ligand hydrogen bonds. The activity of this compound does suggest that positively charged groups may be acceptable in the P1 site. For boceprevir, the dimethylcyclopropyl subunit is predicted to sit in P1, the side chain with the cyclobutyl and terminal ketoamide groups is in P1', the proximal *tert*-butyl group is in P2, the distal *tert*-butyl group is in the hydrophobic pocket at P4/P5, and there are hydrogen bonds with the NH of Gly143, the carbonyl oxygen of Thr26, and three for the urea group with the NH group of Glu166 and the side chain carbonyl of Gln166. All computed poses are for noncovalent docking; few known drugs have sufficiently electrophilic sites to serve as warheads for covalent docking, so this was not pursued. However, there is a crystal structure that has been deposited in the Protein Databank (ID 6WNP) for a boceprevir–M<sup>pro</sup> complex covalently linked to Cys145 at the keto group adjacent to the terminal amide group.<sup>34</sup> This anchoring causes the cyclobutylmethyl and dimethylcyclopropyl groups to sit in P1 and P2, respectively, and the urea-containing appendage with the two *tert*-butyl groups to lie in the P3–P5 region. The docked noncovalent structure is compelling, and it was the 10th best ranked compound with a Glide SP score of –9.5. The orientational difference with the crystal structure for the covalent complex is interesting and may represent a noncovalent binding mode on the pathway to the covalent attachment.

In summary, the present virtual screening study was highly successful in identifying 14 known drugs as showing inhibitory effect on the main protease of SARS-CoV-2. The consensus scoring approach using three docking programs and four protocols was effective in narrowing down ca. 2000 candidate drugs to 42 of high interest. The final 17 compounds that were selected for assay did reflect additional human visualization and

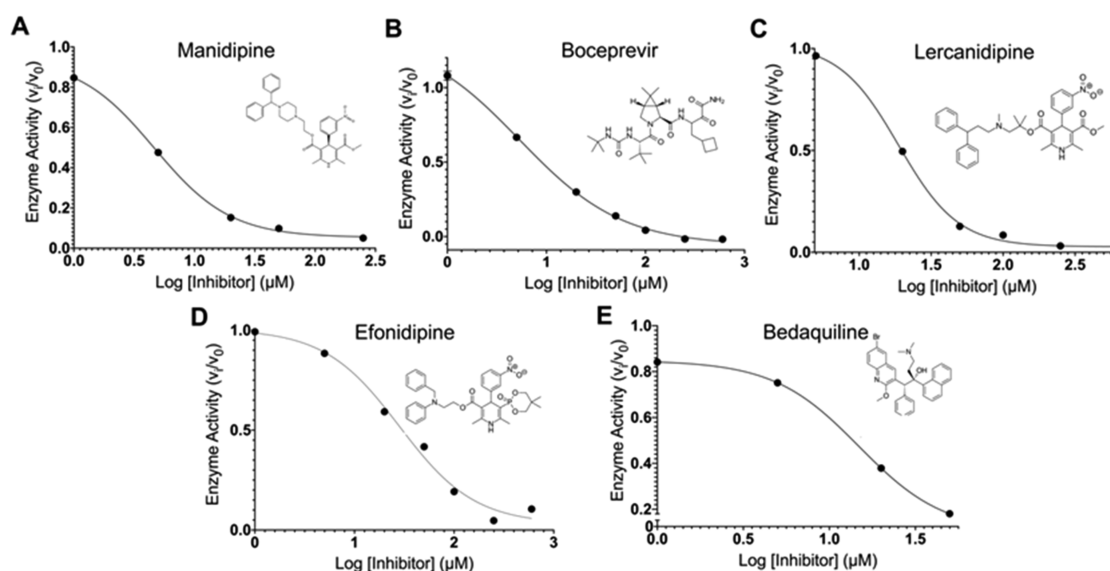


**Figure 6.** IC<sub>50</sub> plots and values for the top five compounds active against SARS-CoV-2 M<sup>pro</sup> from *in vitro* FRET-based assay. IC<sub>50</sub> plots were generated from averaged kinetic data in triplicate for (A) manidipine, (B) boceprevir, (C) lercanidipine, (D) efonidipine, and (E) bedaquiline.



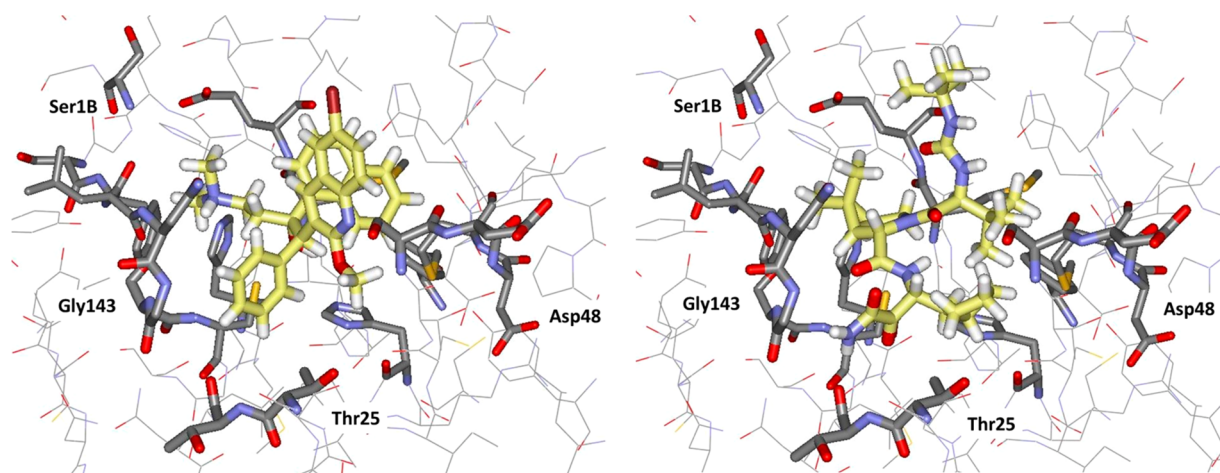


**Figure 7.** Renderings of Glide docking poses for bedaquiline (left) and boceprevir (right).

analyses. Five compounds were identified with  $IC_{50}$  values below  $40\ \mu\text{M}$  with manidipine, boceprevir, lercanidipine, and bedaquiline below  $20\ \mu\text{M}$  at 4.8, 5.4, 16.2, and  $18.7\ \mu\text{M}$ , respectively. Such potencies are very successful for a virtual screening exercise but likely insufficient for repurposing. However, all of the active compounds reported here may provide a foundation for lead optimization to deliver valuable chemotherapeutics to combat the COVID-19 pandemic.

## ■ ASSOCIATED CONTENT

### Supporting Information

The Supporting Information is available free of charge at <https://pubs.acs.org/doi/10.1021/acsmmedchemlett.0c00521>.

Details on the docking calculations, a figure comparing docking scores, details on the MD simulations and results, and a figure with kinetic data for the assays of the five most active compounds (PDF)

Names and docking scores for the full drug library (XLSX)

## ■ AUTHOR INFORMATION

### Corresponding Authors

**Karen S. Anderson** – Department of Pharmacology and Department of Molecular Biophysics and Biochemistry, Yale University School of Medicine, New Haven, Connecticut 06520-8066, United States; [orcid.org/0000-0003-3433-0780](https://orcid.org/0000-0003-3433-0780); Email: [karen.anderson@yale.edu](mailto:karen.anderson@yale.edu)

**William L. Jorgensen** – Department of Chemistry, Yale University, New Haven, Connecticut 06520-8107, United States; [orcid.org/0000-0002-3993-9520](https://orcid.org/0000-0002-3993-9520); Email: [william.jorgensen@yale.edu](mailto:william.jorgensen@yale.edu)

### Authors

**Mohammad M. Ghahremanpour** – Department of Chemistry, Yale University, New Haven, Connecticut 06520-8107, United States; [orcid.org/0000-0002-1129-6041](https://orcid.org/0000-0002-1129-6041)

**Julian Tirado-Rives** – Department of Chemistry, Yale University, New Haven, Connecticut 06520-8107, United States; [orcid.org/0000-0001-7330-189X](https://orcid.org/0000-0001-7330-189X)

**Maya Deshmukh** – Department of Pharmacology, Yale University School of Medicine, New Haven, Connecticut 06520-8066, United States

**Joseph A. Ippolito** – Department of Chemistry, Yale University, New Haven, Connecticut 06520-8107, United States;

Department of Pharmacology, Yale University School of Medicine, New Haven, Connecticut 06520-8066, United States

**Chun-Hui Zhang** – Department of Chemistry, Yale University, New Haven, Connecticut 06520-8107, United States

**Israel Cabeza de Vaca** – Department of Chemistry, Yale University, New Haven, Connecticut 06520-8107, United States

**Maria-Elena Liosi** – Department of Chemistry, Yale University, New Haven, Connecticut 06520-8107, United States

Complete contact information is available at:

<https://pubs.acs.org/doi/10.1021/acsmmedchemlett.0c00521>

## Notes

The authors declare no competing financial interest.

## ■ ACKNOWLEDGMENTS

Gratitude is expressed for support to the U.S. National Institutes of Health (GM32136) and to the Yale University School of Medicine for a CoReCT Pilot Grant. The M<sup>pro</sup> plasmid was kindly provided by the Hilgenfeld lab.<sup>5</sup>

## ■ REFERENCES

- (1) Wu, F.; Zhao, S.; Yu, B.; Chen, Y.-M.; Wang, W.; Song, Z.-G.; Hu, Y.; Tao, Z.-W.; Tian, J.-H.; Pei, Y.-Y.; Yuan, M.-L.; Zhang, Y.-L.; Dai, F.-H.; Liu, Y.; Wang, Q.-M.; Zheng, J.-J.; Xu, L.; Holmes, E. C.; Zhang, Y.-Z. A New Coronavirus Associated with Human Respiratory Disease in China. *Nature* **2020**, *579*, 265–269.
- (2) Jin, Z.; Du, X.; Xu, Y.; Deng, Y.; Liu, M.; Zhao, Y.; Zhang, B.; Li, X.; Zhang, L.; Peng, C.; Duan, Y.; Yu, J.; Wang, L.; Yang, K.; Liu, F.; Jiang, R.; Yang, X.; You, T.; Liu, X.; Yang, X.; Bai, F.; Liu, H.; Liu, X.; Guddat, L. W.; Xu, W.; Xiao, G.; Qin, C.; Shi, Z.; Jiang, H.; Rao, Z.; Yang, H. Structure of Mpro from SARS-CoV-2 and Discovery of Its Inhibitors. *Nature* **2020**, *582*, 289–293.
- (3) Drosten, C.; Günther, S.; Preiser, W.; van der Werf, S.; Brodt, H.-R.; Becker, S.; Rabenau, H.; Panning, M.; Kolesnikova, L.; Fouchier, R. A. M.; Berger, A.; Burguière, A.-M.; Cinatl, J.; Eickmann, M.; Escρίου, N.; Grywna, K.; Kramme, S.; Manuguerra, J.-C.; Müller, S.; Rickerts, V.; Stürmer, M.; Vieth, S.; Klenk, H.-D.; Osterhaus, A. D. M. E.; Schmitz, H.; Doerr, H. W. Identification of a Novel Coronavirus in Patients with Severe Acute Respiratory Syndrome. *N. Engl. J. Med.* **2003**, *348*, 1967–1976.
- (4) Jin, Z.; Zhao, Y.; Sun, Y.; Zhang, B.; Wang, H.; Wu, Y.; Zhu, Y.; Zhu, C.; Hu, T.; Du, X.; Duan, Y.; Yu, J.; Yang, X.; Yang, X.; Yang, K.; Liu, X.; Guddat, L. W.; Xiao, G.; Zhang, L.; Yang, H.; Rao, Z. Structural

Basis for the Inhibition of SARS-CoV-2 Main Protease by Antineoplastic Drug Carmofur. *Nat. Struct. Mol. Biol.* **2020**, *27*, 529–532.

(5) Zhang, L.; Lin, D.; Sun, X.; Curth, U.; Drosten, C.; Sauerhering, L.; Becker, S.; Rox, K.; Hilgenfeld, R. Crystal Structure of SARS-CoV-2 Main Protease Provides a Basis for Design of Improved  $\alpha$ -Ketoamide Inhibitors. *Science* **2020**, *368*, 409–412.

(6) Gimeno, A.; Mestres-Truyol, J.; Ojeda-Montes, M. J.; Macip, G.; Saldivar-Espinoza, B.; Cereto-Massagué, A.; Pujadas, G.; Garcia-Vallvé, S. Prediction of Novel Inhibitors of the Main Protease (M-pro) of SARS-CoV-2 through Consensus Docking and Drug Reposition. *Int. J. Mol. Sci.* **2020**, *21*, 3793.

(7) Ma, C.; Sacco, M. D.; Hurst, B.; Townsend, J. A.; Hu, Y.; Szeto, T.; Zhang, X.; Tarbet, B.; Marty, M. T.; Chen, Y.; Wang, J. Boceprevir, GC-376, and Calpain Inhibitors II, XII Inhibit SARS-CoV-2 Viral Replication by Targeting the Viral Main Protease. *Cell Res.* **2020**, *30*, 678–692.

(8) Morse, J. S.; Lalonde, T.; Xu, S.; Liu, W. R. Learning from the Past: Possible Urgent Prevention and Treatment Options for Severe Acute Respiratory Infections Caused by 2019-nCoV. *ChemBioChem* **2020**, *21*, 730–738.

(9) Pushpakom, S.; Iorio, F.; Eyers, P. A.; Escott, K. J.; Hopper, S.; Wells, A.; Doig, A.; Williams, T.; Latimer, J.; McNamee, C.; Norris, A.; Sanseau, P.; Cavalla, D.; Pirmohamed, M. Drug Repurposing: Progress, Challenges and Recommendations. *Nat. Rev. Drug Discovery* **2019**, *18*, 41–58.

(10) Elfiky, A.; Anti-HCV, A. Nucleotide Inhibitors, Repurposing against COVID-19. *Life Sci.* **2020**, *248*, 117477.

(11) Choy, K.-T.; Wong, A. Y.-L.; Kaewpreedee, P.; Sia, S. F.; Chen, D.; Hui, K. P. Y.; Chu, D. K. W.; Chan, M. C. W.; Cheung, P. P.-H.; Huang, X.; Peiris, M.; Yen, H.-L. Remdesivir, Lopinavir, Emetine, and Homoharringtonine Inhibit SARS-CoV-2 Replication in Vitro. *Antiviral Res.* **2020**, *178*, 104786.

(12) Wang, Y.; Zhang, D.; Du, G.; Du, R.; Zhao, J.; Jin, Y.; Fu, S.; Gao, L.; Cheng, Z.; Lu, Q.; Hu, Y.; Luo, G.; Wang, K.; Lu, Y.; Li, H.; Wang, S.; Ruan, S.; Yang, C.; Mei, C.; Wang, Y.; Ding, D.; Wu, F.; Tang, X.; Ye, X.; Ye, Y.; Liu, B.; Yang, J.; Yin, W.; Wang, A.; Fan, G.; Zhou, F.; Liu, Z.; Gu, X.; Xu, J.; Shang, L.; Zhang, Y.; Cao, L.; Guo, T.; Wan, Y.; Qin, H.; Jiang, Y.; Jaki, T.; Hayden, F. G.; Horby, P. W.; Cao, B.; Wang, C. Remdesivir in Adults with Severe COVID-19: A Randomised, Double-Blind, Placebo-Controlled, Multicentre Trial. *Lancet* **2020**, *395*, 1569–1578.

(13) Costanzo, M.; De Giglio, M. A. R.; Roviello, G. N. SARS CoV-2: Recent Reports on Antiviral Therapies Based on Lopinavir/Ritonavir, Darunavir/Umifenovir, Hydroxychloroquine, Remdesivir, Favipiravir and Other Drugs for the Treatment of the New Coronavirus. *Curr. Med. Chem.* **2020**, *27*, 4536–4541.

(14) Singh, A. K. Chloroquine and Hydroxychloroquine in the Treatment of COVID-19 with or without Diabetes: A Systematic Search and a Narrative Review with a Special Reference to India and Other Developing Countries. *Diabetes Metab. Syndr.* **2020**, *14*, 241–246.

(15) Yao, X.; Ye, F.; Zhang, M.; Cui, C.; Huang, B.; Niu, P.; Liu, X.; Zhao, L.; Dong, E.; Song, C.; Zhan, S.; Lu, R.; Li, H.; Tan, W.; Liu, D. In Vitro Antiviral Activity and Projection of Optimized Dosing Design of Hydroxychloroquine for the Treatment of Severe Acute Respiratory Syndrome Coronavirus 2 (SARS-CoV-2). *Clin. Infect. Dis.* **2020**, *71*, 732–739.

(16) Geleris, J.; Sun, Y.; Platt, J.; Zucker, J.; Baldwin, M.; Hripcsak, G.; Labella, A.; Manson, D. K.; Kubin, C.; Barr, R. G.; Sobieszczyk, M. E.; Schluger, N. W. Observational Study of Hydroxychloroquine in Hospitalized Patients with COVID-19. *N. Engl. J. Med.* **2020**, *382*, 2411–2418.

(17) Hann, M. M. Molecular Obesity, Potency, and Other Addictions in Drug Discovery. *MedChemComm* **2011**, *2*, 349–355.

(18) Fearon, D.; Powell, A. J.; Douangamath, A.; Owen, C. D.; Wild, C.; Krojer, T.; Lukacik, P.; Strain-Damerell, C. M.; Walsh, M. A.; von Delft, F. PanDDA analysis of COVID-19 main protease against the DSI-poised Fragment Library. PDB ID: SR82.

(19) Word, J. M.; Lovell, S. C.; Richardson, J. S.; Richardson, D. C. Asparagine and Glutamine: Using Hydrogen Atom Contacts in the Choice of Side-Chain Amide Orientation. *J. Mol. Biol.* **1999**, *285*, 1735–1747.

(20) Olsson, M. H. M.; Søndergaard, C. R.; Rostkowski, M.; Jensen, J. H. PROPKA3: Consistent Treatment of Internal and Surface Residues in Empirical  $pK_a$  Predictions. *J. Chem. Theory Comput.* **2011**, *7*, 525–537.

(21) Gordon, J. C.; Myers, J. B.; Folta, T.; Shoja, V.; Heath, L. S.; Onufriev, A. H++. A Server for Estimating PKas and Adding Missing Hydrogens to Macromolecules. *Nucleic Acids Res.* **2005**, *33*, 368–371.

(22) Anandakrishnan, R.; Aguilar, B.; Onufriev, A. V. H++ 3.0: Automating PK Prediction and the Preparation of Biomolecular Structures for Atomistic Molecular Modeling and Simulations. *Nucleic Acids Res.* **2012**, *40*, 537–541.

(23) Pettersen, E. F.; Goddard, T. D.; Huang, C. C.; Couch, G. S.; Greenblatt, D. M.; Meng, E. C.; Ferrin, T. E. UCSF Chimera: A Visualization System for Exploratory Research and Analysis. *J. Comput. Chem.* **2004**, *25*, 1605–1612.

(24) Pronk, S.; Páll, S.; Schulz, R.; Larsson, P.; Bjelkmar, P.; Apostolov, R.; Shirts, M. R.; Smith, J. C.; Kasson, P. M.; van der Spoel, D.; Hess, B.; Lindahl, E. GROMACS 4.5: A High-Throughput and Highly Parallel Open Source Molecular Simulation Toolkit. *Bioinformatics* **2013**, *29*, 845–854.

(25) Robertson, M. J.; Tirado-Rives, J.; Jorgensen, W. L. Improved Peptide and Protein Torsional Energetics with the OPLS-AA Force Field. *J. Chem. Theory Comput.* **2015**, *11*, 3499–3509.

(26) Jorgensen, W. L.; Chandrasekhar, J.; Madura, J. D.; Impey, R. W.; Klein, M. L. Comparison of Simple Potential Functions for Simulating Liquid Water. *J. Chem. Phys.* **1983**, *79*, 926–935.

(27) Jorgensen, W. L.; Tirado-Rives, J. Potential Energy Functions for Atomic-Level Simulations of Water and Organic and Biomolecular Systems. *Proc. Natl. Acad. Sci. U. S. A.* **2005**, *102*, 6665–6670.

(28) Jorgensen, W. L.; Tirado-Rives, J. Molecular Modeling of Organic and Biomolecular Systems Using BOSS and MCPRO. *J. Comput. Chem.* **2005**, *26*, 1689–1700.

(29) Dodda, L. S.; Cabeza de Vaca, I.; Tirado-Rives, J.; Jorgensen, W. L. LigParGen Web Server: An Automatic OPLS-AA Parameter Generator for Organic Ligands. *Nucleic Acids Res.* **2017**, *45*, 331–336.

(30) Dai, W.; et al. Structure-based Design of Antiviral Drug Candidates Targeting the SARS-CoV-2 Main Protease. *Science* **2020**, *368*, 1331–1335.

(31) Pillaiyar, T.; Manickam, M.; Namasivayam, V.; Hayashi, Y.; Jung, S.-H. An Overview of Severe Acute Respiratory Syndrome – Coronavirus (SARS-CoV) 3CL Protease Inhibitors: Peptidomimetics and Small Molecule Chemotherapy. *J. Med. Chem.* **2016**, *59*, 6595–6628.

(32) Danta, C. C. Calcium Channel Blockers: A Possible Potential Therapeutic Strategy for the Treatment of Alzheimer's Dementia Patients with SARS-CoV-2 Infection. *ACS Chem. Neurosci.* **2020**, *11*, 2145–2148.

(33) Vatansever, E. C.; Yang, K.; Kratch, K. C.; Drelich, A.; Cho, C. C.; Mellot, D. M.; Xu, S.; Tseng, C. K.; Liu, W. R. Targeting the SARS-CoV-2 Main Protease to Repurpose Drugs for COVID-19. *bioRxiv* **2020**, May 23:2020.05.23.112235. DOI: 10.1101/2020.05.23.112235.

(34) Anson, B.; Mesecar, A. X-ray Structure of SARS-CoV-2 Main Protease Bound to Boceprevir at 1.45 Å. PDB ID: 6WNP. DOI: 10.2210/pdb6wnp/pdb.